Bull. Mater. Sci. (2018) 41:119
https://doi.org/10.1007/s12034-018-1633-z

Synthesis of Chevrel phase ($Cu_{1.8}Mo_6S_8$) in composite with molybdenum carbide for hydrogen evolution reactions

KASINATH OJHA[1], SHIVALI BANERJEE[1], MANU SHARMA[2], PREETI DAGAR[2] and ASHOK K GANGULI[1,2,*]

[1]Department of Chemistry, Indian Institute of Technology Delhi, Hauz Khas, New Delhi 110016, India
[2]Institute of Nano Science and Technology, Habitat Center, Phase 10, Sector 64, Mohali 160062, India
*Author for correspondence (ashok@chemistry.iitd.ac.in)

MS received 10 March 2018; accepted 28 May 2018; published online 30 August 2018

Abstract. Sustainable hydrogen generation from water electrolysis using renewable energy sources is the most promising pathway for future energy and hydrogen economy. Here, the Chevrel phase ($Cu_{1.8}Mo_6S_8$) was synthesized in composite with Mo_2C and good hydrogen evolution activity in acidic media has been demonstrated. Bundles of nanowires were formed in the templated synthesis route. The composites were characterized by X-ray diffraction, transmission electron microscopy, scanning electron microscopy and elemental analysis. Detailed electrochemical analysis reveals that MCS-Cu50 composite exhibits higher hydrogen evolution reaction (HER) activity with 71.4 mA cm^{-2} current density at an overpotential of 400 mV. It requires 250 mV overpotential to produce 10 mA cm^{-2} current density for HER.

Keywords. $Cu_{1.8}Mo_6S_8$; Chevrel phase; molybdenum carbide; hydrogen evolution reactions.

1. Introduction

Energy is the most important input for the social and economic development of a country. As an outcome of the generalization of agricultural, industrial and domestic activities the demand for energy has increased remarkably worldwide. The increasing demand for energy has forced people to exploit the natural resources (coal, petroleum, etc.) in an uncontrollable manner. Due to the present condition of the environment, there is an urgent need to completely switch over from non-renewable sources of energy to the renewable sources. This is the main driving force behind the efforts to utilize renewable energy sources more effectively. Renewable energy basically includes the electricity and heat generated from solar, wind, ocean, hydropower, biomass, geothermal resources, bio-fuels and hydrogen derived from renewable resources. Hydrogen would be ideal as a synthetic fuel because it is light weight and can be obtained in abundance by the electrochemical splitting of water. Platinum is one of the best electrocatalysts for hydrogen evolution reaction (HER). The scarcity and very high cost of platinum metal has led to an intensive research to develop electrocatalysts for HER. Mo-based compounds have gained much importance as an alternative for platinum in HER. Notable recent progress has been made in the past decade in developing acid-stable HER catalysts, resulting in the discovery of excellent HER activity for MoS_2, Mo_2C, MoB, Ni–Mo, Ni–Mo–N and Ni_2P, which all contain Mo and/or Ni [1–9]. Various reports exist wherein transition metal carbides [10–12], nitrides [4,13–15], phosphides [7,16–18] and sulphides [19–22] are found to be used as a replacement for platinum as an electrocatalyst for hydrogen evolution reaction. Molybdenum compounds possess downward shift in the d band centre with respect to the Fermi level and the anti-bonding state is below the Fermi level, which decreases the hydrogen binding energy and results in weaker M–H_{ad} bond [14,23]. Hence desorption of hydrogen from the surface of the electrocatalyst becomes easy and this enhances the efficiency of the catalyst.

Metal-ion-doped molybdenum-based compounds were explored for good HER activity. Co-doped Mo_2C nanowires were demonstrated for good HER activity with η_{10} of 140 mV, where Co doping increases the electron density at the Fermi level and results in weaker M–H bond [24]. This in turn facilitates the HER activity. Co-doped nickel phosphide was exhibited as a good HER catalyst, where Co doping results in moderate H adsorption and facilitates H_2 release from the catalyst's surface [25]. Cu doping in CoS_2 results in remarkable HER activity [26] of η_{10} at an overpotential of 52 mV with a Tafel slope of 42 mV dec^{-1} and large exchange current density of 0.68 mA cm^{-2}. Cu doping leads to lower H adsorption energy and awakens the inert S sites for HER activity [26]. Cu-doped Ni catalyst exhibits HER activity of 10 mA cm^{-2} at an overpotential of 27 mV with a small Tafel slope of 33.3 mV dec^{-1} in 1 M KOH solution [27]. Mo-based

Electronic supplementary material: The online version of this article (https://doi.org/10.1007/s12034-018-1633-z) contains supplementary material, which is available to authorized users.

sulphides exhibit remarkable HER activity [22,28–30]. However, Cu, Mo-based sulphides (Chevrel phase) were not explored for electrochemical HER activity. Here, we have synthesized a Cu-based Chevrel phase ($Cu_{1.8}Mo_6S_8$) in composite with Mo_2C. Introduction of Cu ions in the reaction of Mo_2C–MoS_2 leads to Chevrel phase formation. This composite was explored for electrochemical hydrogen evolution in acidic media and it exhibits good HER activity.

2. Experimental

2.1 *Materials*

Ammonium molybdate tetrahydrate (CDH Chemicals), copper (II) nitrate hydrate (BDH), trithiocyanuric acid (Alfa Aesar) and aniline (Qualigens) were used without any further purification. Nafion was purchased from Sigma Aldrich. Double-distilled water was used in all the experiments.

2.2 *Synthesis of Mo_2C–$Cu_{1.8}Mo_6S_8$*

To synthesize the composites, a two-step reaction was carried out where, in the first step, ammonium molybdate was converted into anilinium molybdate via complex formation with aniline and then in the second step, the complex material (precursor) was annealed at 800°C in argon atmosphere as reported earlier [10]. Here, we introduce trithiocyanuric acid as a sulphur source to get carbide- and sulphide-based composites. In brief, 1 mmol of ammonium molybdate, 1 mmol of trithiocyanuric acid and 50 ml double-distilled water were taken in a beaker. The mixture was kept on a stirrer for half an hour and then 1 ml of aniline was added to the mixture under stirring followed by addition of dilute HCl dropwise in order to obtain a pH of 3.5. After that the mixture was kept at around 50°C overnight to get the precipitate of ammonium anilinium molybdate complex. The precipitate was filtered and dried. The product was ground and heated at 800°C for 5 h. This reaction was repeated by adding a certain percentage of Cu(II) nitrate with ammonium molybdate (copper mole percentage of 5, 10, 25, 50 and 75). 100% Cu containing reaction was carried out as a control reaction without any Mo ions. Exact reaction compositions are given in supplementary table S1.

2.3 *Characterization*

The crystallinity, phase composition and purity of the resulting nanocomposites were assessed through X-ray diffraction (XRD) analysis on a Bruker D8 Advance diffractometer equipped with Ni-filtered Cu Kα radiation ($\lambda = 1.5418$ Å) in the 2θ range of 10–80° at a scanning rate of 0.02° s^{-1}. The surface morphologies of the composites were analysed by scanning electron microscopy (SEM, JEOL IT300) operating at an accelerating voltage of 15 kV. Transmission electron microscopy (TEM) studies were carried out using a Technai G^2 20 electron microscope operated at 200 kV. TEM specimens were prepared by dispersing the nanocomposites in ethanol by ultrasonic treatment, dropping onto a porous carbon film supported on a copper grid and then drying in air.

2.4 *Electrochemical measurements*

Linear sweep voltammetry (LSV), cyclic voltammetry (CV) and electrochemical impedance spectroscopic measurements were carried out with a computer-controlled electrochemical workstation (Autolab PGSTAT 302 N). Hydrogen evolution reactions were studied using three-electrode set-ups where Ag–AgCl, graphite rod and catalyst-coated glassy carbon electrode (GCE) were used as the reference electrode, counter-electrode and working electrode, respectively. The sample preparation methodology is as follows: a slurry was obtained by dispersing 2.5 mg of Mo_2C–$Cu_{1.8}Mo_6S_8$ nanocomposite in 480 µl of isopropanol and 20 µl of Nafion; 2 µl of this slurry was carefully drop-casted on the working electrode and dried for 10 min. Nafion acts as a proton-conducting binder for nanoparticles, which forms a membrane over the surface of the electrode. All the three electrodes were placed in a freshly prepared solution of 0.5 M H_2SO_4. LSV was carried out at a scan rate of 5 mV s^{-1} in the potential range of (0 to −0.6 V). CV was carried out at different scan rates in the potential range of +0.04 to +0.4 V *vs.* RHE. Electrochemical impedance spectroscopic measurements were carried out over 100 kHz–0.1 Hz at a particular applied bias. All potentials have been reported with respect to that of reversible hydrogen electrode (RHE).

3. Results and discussion

3.1 *Synthesis and structural analysis*

The composites were synthesized in a two-step reaction where, in the first step, ammonium molybdate was converted into anilinium ammonium molybdate via complex formation with aniline and then in the second step, the complex material (precursor) was annealed at 800°C in argon atmosphere, which led to the formation of Mo_2C–$Cu_{1.8}Mo_6S_8$ composites. This synthesis route was used to synthesize Mo_2C and Mo_2N nanostructures [13,31] earlier. Here, trithiocyanuric acid was used as the S source to get MoS_2 along with Mo_2C. Introduction of Cu ions in the reaction mixture led to the formation of Chevrel phase ($Cu_{1.8}Mo_6S_8$) along with Mo_2C. The phase formation and structures were identified from the XRD analysis. The reaction of anilinium molybdate complexes (precursor) with trithiocyanuric acid at 800°C led to the formation of amorphous Mo_2C and MoS_2 as confirmed by the powder XRD (figure 1). When Cu ions are added to the reaction mixture, it results in the Chevrel phase ($Cu_{1.8}Mo_6S_8$, JCPDS no-840239) formation along with Mo_2C (orthorhombic structure, JCPDS no-790744). With increase in the Cu content, the Chevrel

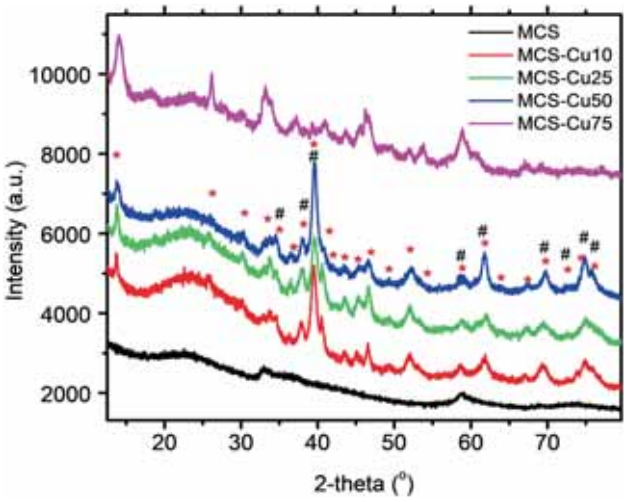

Figure 1. Powder XRD pattern of Mo_2C–$Cu_{1.8}Mo_6S_8$ (# is Mo_2C and * is Chevrel phase $Cu_{1.8}Mo_6S_8$).

phase formation increases and at the same time Mo_2C phase decreases. At 75% of Cu content (MCS-Cu75), Chevrel phase ($Cu_{1.8}Mo_6S_8$) was formed with negligible amount of Mo_2C. However, the XRD pattern (supplementary figure S1) of the control reaction containing 100% Cu shows the formation of Cu_2S (tetragonal structure, JCPDS no-721071).

3.2 *Microscopic and elemental analysis of Mo_2C–$Cu_{1.8}Mo_6S_8$ composites*

In figure 2, SEM micrographs show that flakes and bundle of nanowires are obtained, which may be due to the template of the precursor (anilinium molybdate complex) as evident in the earlier reports [10]. The Chevrel-phase-based composites exhibit morphologies having bundles of nanowires (figure 2).

The SEM micrograph of the product of the control reaction with 100% Cu shows the presence of cluster of particles with random morphology (figure 2f), which might be due to the formation of Cu_2S as confirmed from the powder XRD analysis (supplementary figure S1). EDAX analysis of the sample (MCS-Cu50) confirms the presence of Cu, Mo, C and S in the composites (figure 3a). The variation in the ratio of Cu and Mo is confirmed from the EDAX quantification (supplementary table S2). In the absence of copper (in case of MCS), Mo_2C and MoS_2 composite was formed. The presence of copper in the reaction system results in the Chevrel phase along with Mo_2C minor phase formation. It was observed that Mo content in the composites decreases with respect to Cu content as expected. Again, S content increases, which indicates higher amount of Chevrel phase formation as Chevrel phase has high S content. This follows the reaction condition where increase in the copper content results in higher amount of Chevrel phase formation. The elemental mapping of one of the composites (MCS-Cu50) suggests that Mo, S and Cu are present uniformly throughout the sample (figure 3b–e). The mapping of carbon shows dark region of the sample area, indicating that the presence of Mo_2C is less compared with Chevrel phase (figure 3d).

TEM images of Mo_2C–MoS_2 composite exhibit nanorod morphologies, which are composed of amorphous Mo_2C nanoparticles and MoS_2 sheets (figure 4a–c). High-resolution TEM images show the layers of MoS_2 randomly oriented in the nanorod morphology as marked in figure 4b and c. In the composite of Mo_2C–$Cu_{1.8}Mo_6S_8$ (MCS-Cu50), nanowires

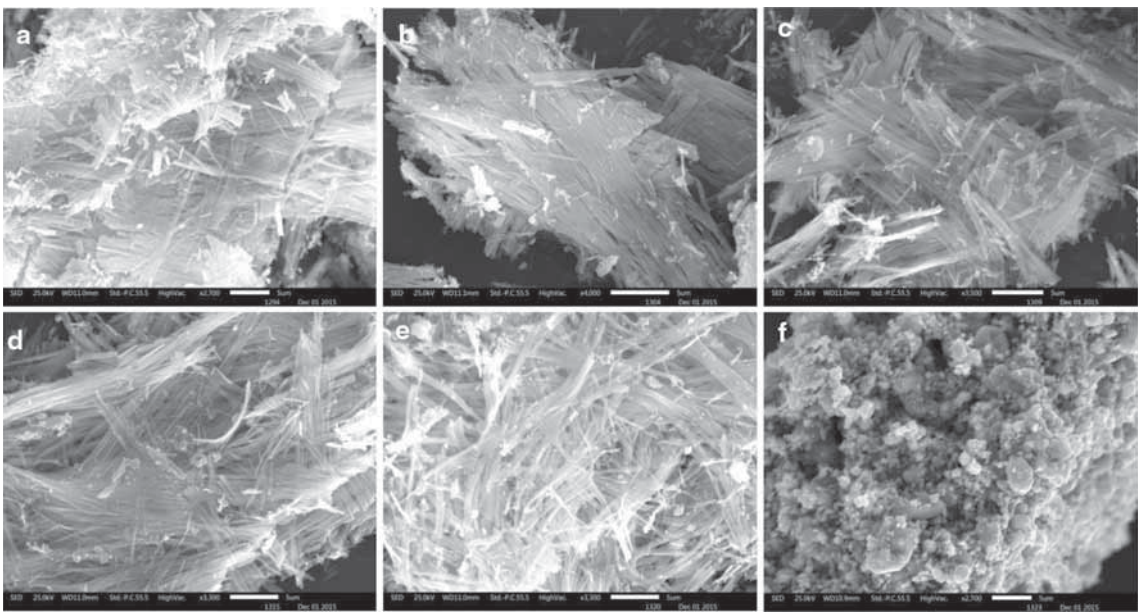

Figure 2. SEM images of Mo_2C–$Cu_{1.8}Mo_6S_8$ composites: (**a**) MCS, (**b**) MCS-Cu10, (**c**) MCS-Cu25, (**d**) MCS-Cu50, (**e**) MCS-Cu75 and (**f**) Cu100.

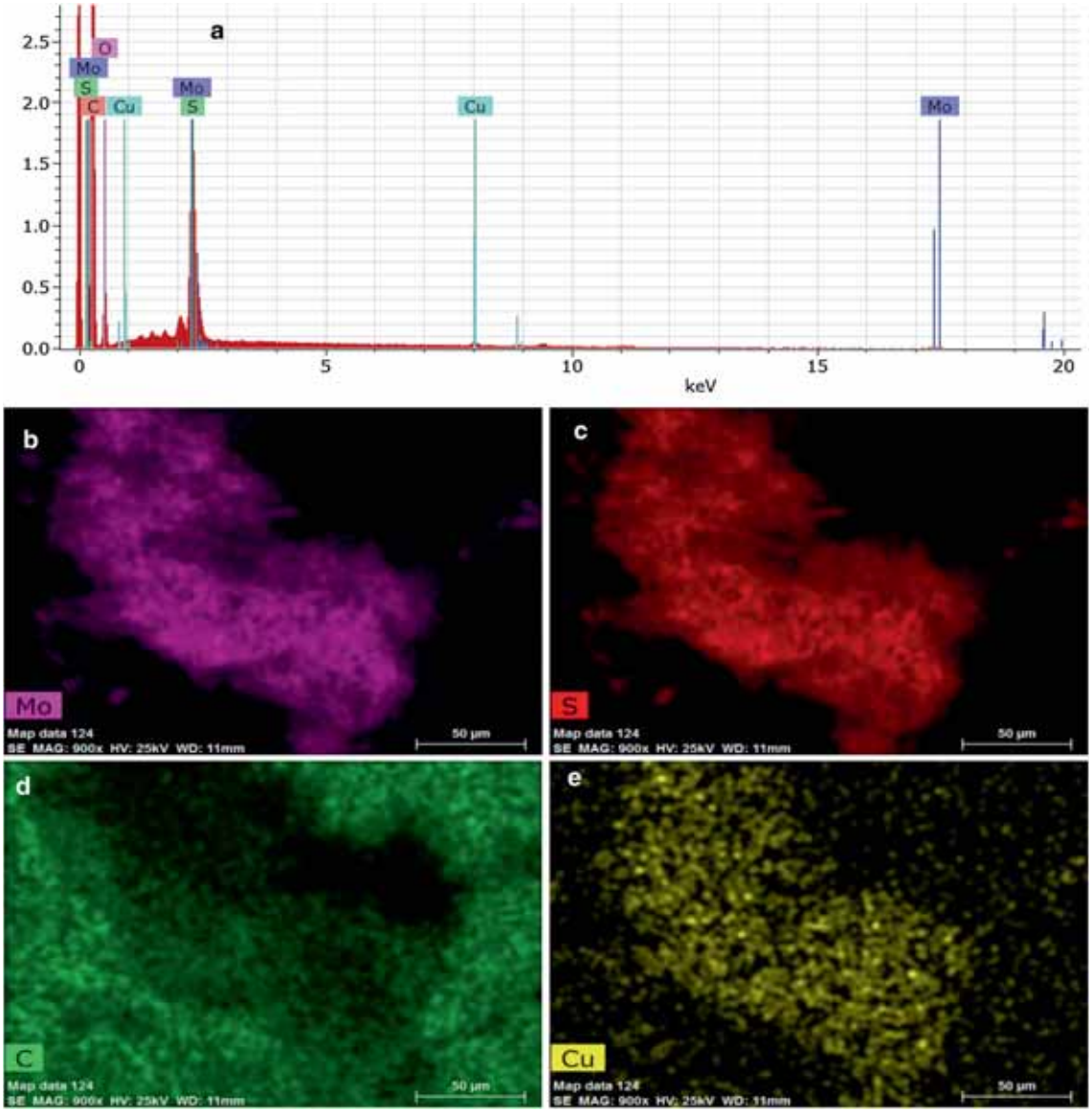

Figure 3. (**a**) EDAX profile and (**b–e**) elemental mapping of MCS-Cu50 showing the presence of the elements.

are evident and are composed of small particles of Chevrel phase along with Mo_2C particles (figure 4d–f). The lattice fringes in the high-resolution TEM image are identified as the (001) plane of $Cu_{1.8}Mo_6S_8$ crystals.

3.3 *Electrochemical analysis*

Electrochemical hydrogen evolution reactions using the Mo_2C–$Cu_{1.8}Mo_6S_8$ composites deposited on GCE with a mass loading of 1.66 mg cm^{-2} have been investigated using a typical three-electrode system in 0.5 M H_2SO_4 aqueous solution.

LSV studies, where current density has been recorded as a function of applied potential at a sweep rate of 5 mV s^{-1}, suggest that these composites exhibit good catalytic activity for hydrogen evolution. LSV curves (figure 5a) show the highest current density (71.4 mA cm^{-2} at −0.4 V *vs.* RHE) for the composite MCS-Cu50, whereas 39.22, 52.02, 66.67 and 70.2 mA cm^{-2} current densities were observed for MCS, MCS-Cu05, MCS-Cu25 and MCS-Cu75 composites, respectively. The current density is found to increase with the increase in the Cu content up to 50%. Further increase in the Cu content decreases the current density. The overpotential required for driving a current density of 10 mA cm^{-2} was found to be 270, 250, 250, 250, 250 and 280 mV for MCS, MCS-Cu05, MCS-Cu10, MCS-Cu25, MCS-Cu50 and MCS-Cu75, respectively (supplementary table S3).

To understand the mechanism of the hydrogen evolution reaction, we have studied upon the Tafel slope values

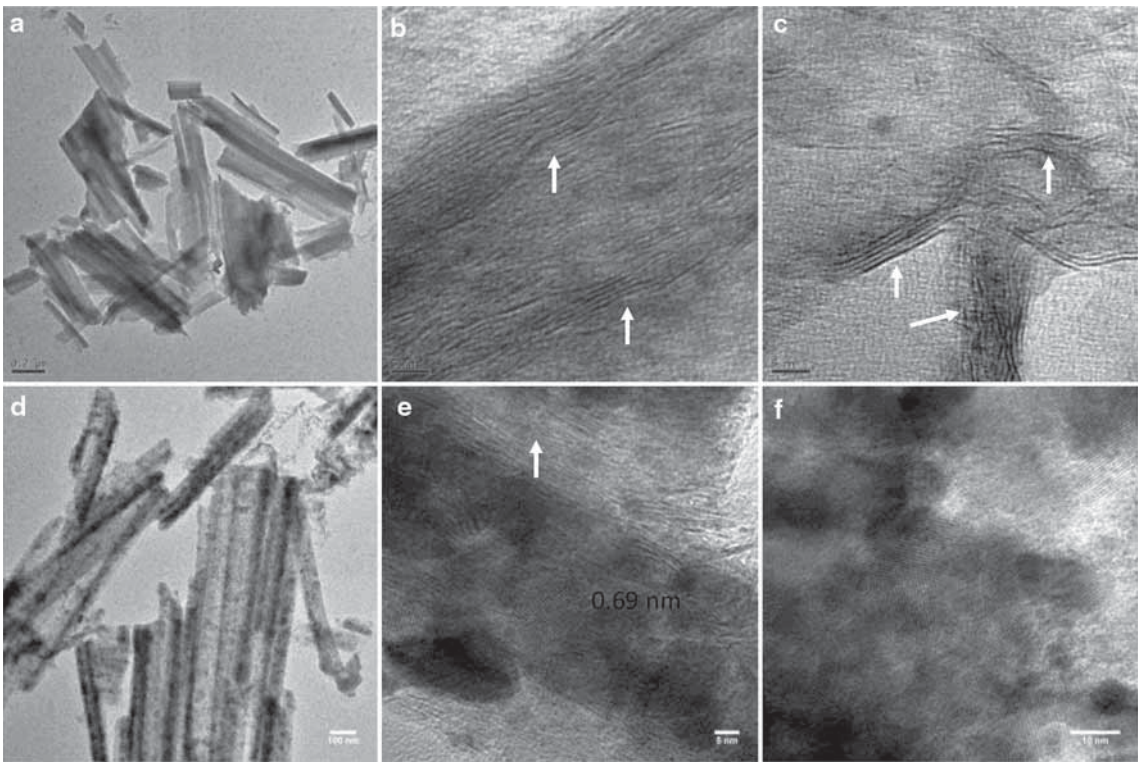

Figure 4. TEM images: (**a**–**c**) Mo_2C–MoS_2 (MCS) and (**d**–**f**) Mo_2C–$Cu_{1.8}Mo_6S_8$ nanocomposite (MCS-Cu50). Arrow indicates the MoS_2 layers in the TEM images.

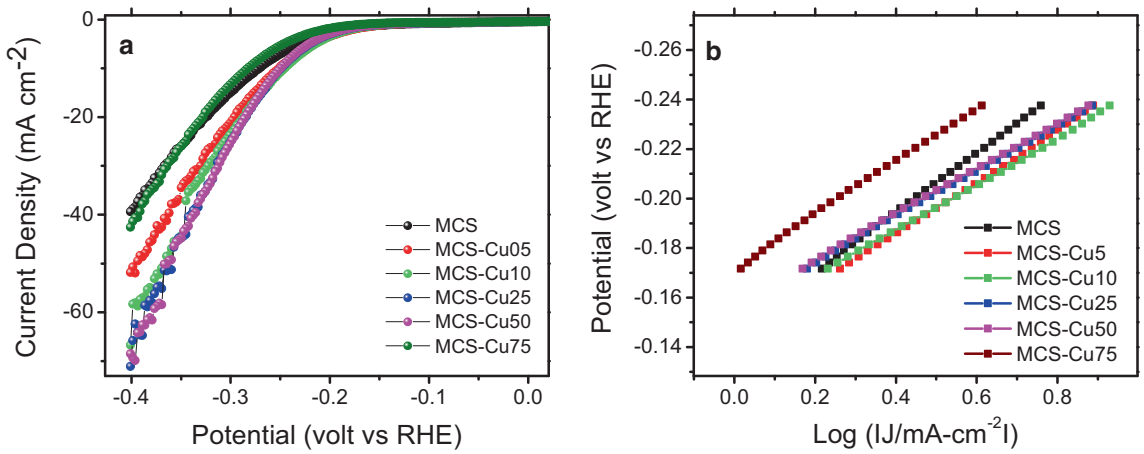

Figure 5. (**a**) LSV curve and (**b**) Tafel slopes of Mo_2C–$Cu_{1.8}Mo_6S_8$ composites.

(figure 5b) of the composites, which is the slope of the overpotential *vs.* log(|current density|) curve and is indicative of the mechanism of the HER process. Tafel slopes were found to be 120, 104, 93, 92, 92 and 109 mV dec^{-1} for MCS, MCS-Cu05, MCS-Cu10, MCS-Cu25, MCS-Cu50 and MCS-Cu75, respectively. The Tafel slope of 120 mV dec^{-1} suggests that Volmer reaction is the rate-limiting step for the hydrogen evolution reaction. However, the Tafel slopes lower than the standard value of 120 mV dec^{-1} indicate that the HER process follows the Volmer–Heyrovsky mechanism with intermediate reaction kinetics. The rate-determining step is transferred to the Heyrovsky reaction from the Volmer process. This implies that the HER process may follow the fast discharge reaction (i.e., Volmer reaction) followed by slow desorption reaction (Heyrovsky reaction). The electrochemically active surface area (ECSA) of the samples was calculated from the CV. CV measurements were carried out at different scan rates in the potential region of 0.05–0.45 V (*vs.* RHE), where no redox peaks were observed (supplementary figure S2). We have calculated the specific capacitance

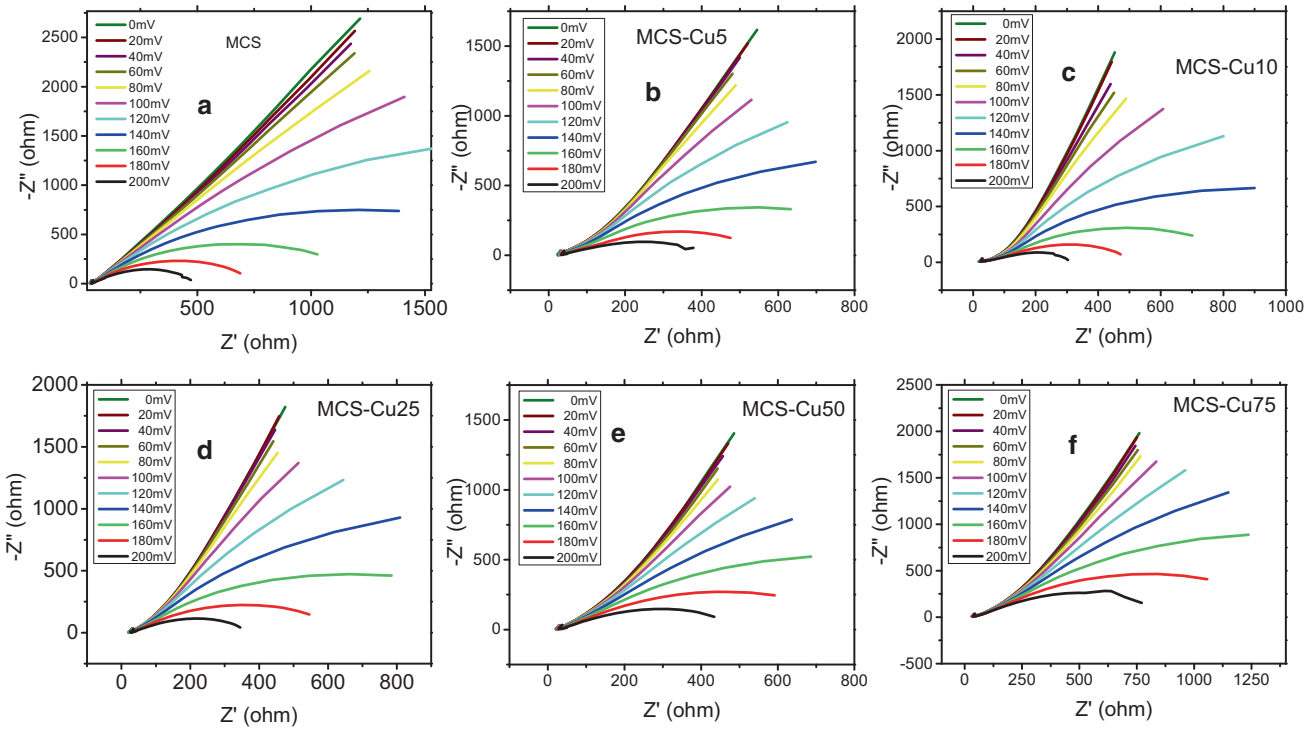

Figure 6. Nyquist plot of Mo_2C–$Cu_{1.8}Mo_6S_8$ composites: (**a**) MCS, (**b**) MCS-Cu05, (**c**) MCS-Cu10, (**d**) MCS-Cu25, (**e**) MCS-Cu50 and (**f**) MCS-Cu75.

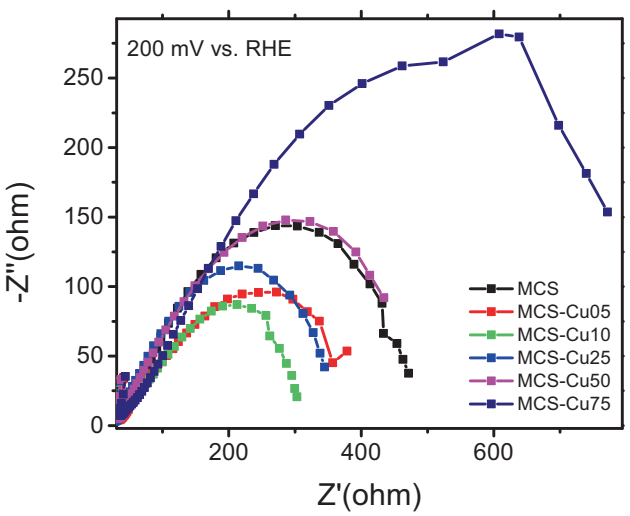

Figure 7. Nyquist plot of Mo_2C–$Cu_{1.8}Mo_6S_8$ composites at an applied bias of 200 mV.

of each composite from the slope of the linear plot of Δj (current density) *vs.* scan rate (supplementary figure S3) at a potential of 0.25 V (*vs.* RHE). The specific capacitance is the double of the slopes. The specific capacitances of 10, 14, 22, 16.5, 21 and 18.5 mF cm^{-2} were found for MCS, MCS-Cu5, MCS-Cu10, MCS-Cu25, MCS-Cu50 and MCS-Cu75, respectively. We used specific capacitance of 40 μF cm^{-2} (a moderate value as reported in a recent report) to calculate ECSA for the electrodes. The ECSA (A_{ECSA}) can be calculated from the following equation:

$$A_{ECSA} = (\text{specific capacitance})/(40\,\mu\text{F cm}^{-2}).$$

Therefore, the highest ECSA was found in the case of MCS-Cu10 composite.

Electrochemical impedance spectroscopic measurements at different applied biases suggest that the charge transfer resistance (R_{ct}) decreases with the applied bias, which implies higher HER activity at higher applied potentials (figure 6). When we compared the Nyquist plot of the composites at a particular applied bias of 200 mV (*vs.* RHE), we found that MCS-Cu10 exhibits a smaller semicircle, i.e., lower R_{ct} indicating higher HER activity of the composite (figure 7).

4. Conclusion

The Mo_2C–$Cu_{1.8}Mo_6S_8$ composites also exhibit good catalytic activity for hydrogen evolution. The current density is found to increase with the increase in the mole percentage of Cu ions (50%) in the reaction mixture. The specific capacitance of each composite has been calculated from the slope of the linear plot of Δj (current density) *vs.* scan rate at a potential of 0.25 V (*vs.* RHE). The highest ECSA was found in the case of MCS-Cu10 composite. Electrochemical impedance spectroscopic measurements at different applied biases suggest that the charge transfer resistance (R_{ct}) decreases with the applied bias, which implies higher HER activity at higher

applied potentials. When the Nyquist plot of the composites was compared at a particular applied bias of 200 mV (*vs.* RHE), it was found that MCS-Cu10 exhibits the lowest R_{ct}, indicating higher HER activity of the composite. However, these composites exhibited 10 mA cm^{-2} current density at an overpotential of 250 mV. Various Chevrel phases can be explored further for HER activity.

Acknowledgements

AKG thanks DST and DeitY, Government of India, for financial support. KO thanks UGC, Government of India, for fellowship. MS and PD thank INST for the fellowship.

References

[1] Xiao P, Yan Y, Ge X, Liu Z, Wang J Y and Wang X 2014 *Appl. Catal. B Environ*. **154–155** 232
[2] Michalsky R, Zhang Y and Peterson A A 2014 *ACS Catal*. **4** 1274
[3] Cao B, Veith G M, Neuefeind J C, Adzic R R and Khalifah P G 2013 *J. Am. Chem. Soc*. **135** 19186
[4] Xie J, Li S, Zhang X, Zhang J, Wang R, Zhang H *et al* 2014 *Chem. Sci*. **5** 4615
[5] Ma L, Ting L R L, Molinari V, Giordano C and Yeo B S 2015 *J. Mater. Chem. A* **3** 8361
[6] Chang J, Feng L, Liu C, Xing W and Hu X 2014 *Energy Environ. Sci*. **7** 1628
[7] Chen X, Wang D, Wang Z, Zhou P, Wu Z and Jiang F 2014 *Chem. Commun*. **50** 11683
[8] Scanlon M D, Bian X, Vrubel H, Amstutz V, Schenk K, Hu X *et al* 2013 *Phys. Chem. Chem. Phys*. **15** 2847
[9] Vrubel H and Hu X 2012 *Angew. Chemie Int. Ed*. **51** 12703
[10] Liao L, Wang S, Xiao J, Bian X, Zhang Y, Scanlon M D *et al* 2014 *Energy Environ. Sci*. **7** 387
[11] Chen W F, Wang C H, Sasaki K, Marinkovic N, Xu W, Muckerman J T *et al* 2013 *Energy Environ. Sci*. **6** 943
[12] Chen W F, Muckerman J T and Fujita E 2013 *Chem. Commun. (Camb.)* **49** 8896
[13] Ojha K, Saha S, Kumar B, Hazra K S and Ganguli A K 2016 *ChemCatChem* **8** 1218
[14] Chen W F, Muckerman J T and Fujita E 2013 *Chem. Commun*. **49** 8896
[15] Liu J, Tang S, Lu Y, Cai G, Liang S, Wang W *et al* 2013 *Energy Environ. Sci*. **6** 2691
[16] Huang Z, Chen Z, Chen Z, Lv C, Humphrey M G and Zhang C 2014 *Nano Energy* **9** 373
[17] Popczun E J, Mckone J R, Read C G, Biacchi A J, Wiltrout A M, Lewis N S *et al* 2013 *J. Am. Chem. Soc*. **135** 9267
[18] Ojha K, Sharma M, Kolev H and Ganguli A K 2017 *Catal. Sci. Technol*. **7** 668
[19] Liao L, Zhu J, Bian X, Zhu L, Scanlon M D, Girault H H *et al* 2013 *Adv. Funct. Mater*. **23** 5326
[20] Li H, Tsai C, Koh A L, Cai L, Contryman A W, Fragapane A H 2015 *et al Nat. Mater*. **15** 48
[21] Jaramillo T F, Jørgensen K P, Bonde J, Nielsen J H, Horch S and Chorkendorff I 2007 *Science* **317** 100
[22] Li G, Zhang D, Qiao Q, Yu Y, Peterson D, Zafar A *et al* 2016 *J. Am. Chem. Soc*. **138** 16632
[23] Paloukis F, Zafeiratos S, Drakopoulos V and Neophytides S G 2008 *Electrochim. Acta* **53** 8015
[24] Lin H, Liu N, Shi Z, Guo Y, Tang Y and Gao Q 2016 *Adv. Funct. Mater*. **26** 5590
[25] Li J, Yan M, Zhou X, Huang Z Q, Xia Z, Chang C R *et al* 2016 *Adv. Funct. Mater*. **26** 6785
[26] Zhang J, Xiao B, Liu X, Liu P, Xi P, Xiao W *et al* 2017 *J. Mater. Chem. A* **5** 17601
[27] Sun Q, Dong Y, Wang Z, Yin S and Zhao C 2018 *Small* **1704137** 1704137
[28] Yu L, Xia B Y, Wang X and Lou X W 2016 *Adv. Mater*. **28** 92
[29] Hinnemann B, Moses P G, Bonde J, Jørgensen K P, Nielsen J H, Horch S *et al* 2005 *J. Am. Chem. Soc*. **127** 5308
[30] Vrubel H, Merki D and Hu X 2012 *Energy Environ. Sci*. **5** 6136
[31] Ojha K, Saha S, Kolev H, Kumar B and Ganguli A K 2016 *Electrochim. Acta* **193** 268